PORE PRESSURE PREDICTION USING 3D SEISMIC VELOCITY DATA: A CASE STUDY, A CARBONATE OIL FIELD, SW IRAN

EHSAN NOSRAT[1], ABDOLRAHIM JAVAHERIAN[1,2], MAHMOUD REZA TORABI[3] and HOMAYOUN BEHZAD ASIRI[4]

1 Department of Mining, Metallurgical and Petroleum Engineering, Amirkabir University of Technology, Tehran, Iran.
2 Institute of Geophysics, University of Tehran, PO Box 14155 6466, Tehran, I.R. Iran.
3 Department of Geophysics, Exploration Directorate of N.I.O.C., Tehran, Iran.
4 Department of Petroleum Engineering, Exploration Directorate of N.I.O.C., Tehran, Iran.
ehsan_nosrat@aut.ac.ir, javaheri@ut.ac.ir, mrtorabi@niocexp.org, basiri@niocexp.org

ABSTRACT

Nosrat, E., Javaherian, A., Torabi, M.R. and Asiri, A.B., 2010. Pore pressure prediction using 3D seismic velocity data: a case study, a carbonate oil field, SW Iran. *Journal of Seismic Exploration*, 19: 141-159.

Pore pressure is an important parameter in hydrocarbon resource exploration and production. Accurate knowledge of the pore pressure is a key requirement for safe and economical planning of wells. Knowledge of formation pressure is not only essential for safe and cost-effective drilling of wells, but also is critical for assessing exploration risk factors including the migration of formation fluids and seal integrity. Pore pressure prediction based on seismic velocity is a common method for pre-drill pore pressure prediction, especially in sandstone reservoirs. In this method, pore pressure can be obtained from transformation of seismic velocity to pore pressure. But seismic velocities need to be derived using methods having sufficient resolution for well planning purposes.

In this study, the velocity derived from pre-stack time migration (PSTM) was available in some parts of the field; however, in another part of the field the only available velocity field was the stacking velocity. This combined velocity field was calibrated with the velocities derived from sonic logs. They were then sorted on regular grid sizes using some geostatistical methods. The effective pressure cube was constructed using the Bowers equation and the calibrated velocity field. The pore pressure cube was constructed by computing the differences between the overburden pressure cube and the effective pressure cube, which was computed using the density cube. Finally the predicted pore pressure cube was calibrated with the measured pore pressures at the locations of 8 wells using geostatistical methods. In a large undeveloped oil field in southwest Iran, some carbonate formations encountered abnormal pressure zones. In the area of study, the combined velocity field was improved and calibrated; then, the pore pressure cube was generated accordingly. The predicted pressures show good agreement with the measured pressures at the 8 well locations.

KEYWORDS: pore pressure prediction, geostatistics, kriging, variography, stacking velocity, effective pressure, Bowers equation, carbonate reservoir.

INTRODUCTION

Abnormal pressure is an important danger during the drilling phase of oil and gas field development. Geopressure is an anomalously high pore fluid pressure in a formation, which is higher than hydrostatic pressure (Kan and Swan, 2001). Overpressures in sedimentary basins are attributed to different mechanisms such as under-compaction or compaction disequilibrium in shale, oil-to-gas conversion; unloading processes, and fluid migration. However, the observed pore pressure is largely attributed to under-compaction (Badri et al., 2000). A large number of methods and formulas, which are used for predicting pore pressure, are based on this theory. The velocity analysis, which is used in seismic data processing, provides a suitable tool for pre-drill pore pressure prediction (Chopra and Huffman, 2006). In this work, it is assumed that the variation of elastic wave velocity with pore pressure and stress follows the effective stress principle (Den Boer et al., 2006). The effective pressure on a reservoir is often defined as the difference between the total overburden pressure and the formation pore pressure (Dutta et al., 2002). Hence, when both the overburden pressure and the formation fluid pressure are varied, only the difference between them has a significant influence on porosity, formation compaction, and velocity (Gregory, 1978). By calibrating the change in the seismic velocity and the effective pressure using some relationships such as Bowers (1995) and Eaton (1975) formulas and using the relationship between pore pressure and effective pressure, we can predict the pore pressure magnitude using seismic velocity. In addition to the effective pressure, other parameters such as rock type and fluid type affect the seismic velocity (Dodds et al., 2007). Accurate pore pressure prediction needs the accurate high resolution velocity field. A good initial velocity model is the key to successful pressure prediction (Kan et al., 1999). The velocities derived from reflection tomography and prestack migrations have enough resolution for accurate pore pressure prediction (Carcione and Helle, 2002). But the stacking velocity does not have enough vertical and lateral resolutions for accurate pore pressure prediction. Conventional seismic velocity analyses assume that the velocity varies slowly both laterally and vertically (Sayers et al., 2002). The final goal of this study is to construct a 3D pore pressure cube.

THE AREA OF STUDY

The area of study is an onshore large oil field in southwest Iran. The sedimentary models of this area show that these sediments belong to carbonate ramps. An important reservoir in this field is the Fahliyan carbonate formation. This formation encounters abnormal pressure. The formation belongs to the Khami group and consists of 365 m massive limestone. The acoustic impedance inversion has shown that this formation consists of isolated reef structures.

Furthermore, it contains very light oil. The depth of burial of this formation may lead to overpressure pockets.

METHODOLOGY

The following steps were taken to predict pore pressure: (1) correcting the available velocity field with respect to velocities derived from sonic logs at the well-locations, using geostatistical methods, due to the better resolution of the velocities derived from wells, (2) calculating overburden pressure by integrating density logs at the wells, (3) calculating effective pressure by taking the differences between the measured pore pressure and the calculated overburden pressure at the well-locations, (4) fitting the Bowers (1995) equation to the velocity versus the effective pressure cross-plot for well-data, (5) fitting Gardner's (1974) relationship between the density and the velocity data at the well-locations and converting the corrected velocity cube to the density cube and integrating the density cube with regard to depth and calculating overburden pressure cube, (6) converting the corrected velocity cube to the effective pressure cube using the fitted Bowers (1995) equation to the well data, (7) calculating the differences between the overburden pressure cube and the effective pressure cube and constructing the initial pore pressure cube, (8) calibrating the initial pore pressure cube with measured pore pressure at the well-locations using geostatistical methods and (9) converting the depth scale to two-way time data by using the check-shot data. Fig. 1 shows the overall flow-diagram for pore pressure prediction in this study.

Available data

The available velocity field data consists of the velocity derived from prestack time migration (PSTM) in a part of the area and the conventional stacking velocity in another part of the area. The grid of the velocity analysis is 500 by 500 m for prestack studies and 2000 by 2000 m for conventional velocity analysis. In addition, the information of the 8 wells was used to predict pore pressures. In these wells, different types of petrophysical logs were available; however, only the sonic and the density logs are required to predict the pore pressure. Furthermore, the check-shot data were available for all the wells. The check-shot data were used for correcting the initial velocity field and converting the depth scale to the two way time scale. Also, the measured pore pressure using RFT/DST tests were available at the wells. In some wells, where the Fahliyan formation encounters abnormal pressures, the pore pressure was measured at different depths for each well.
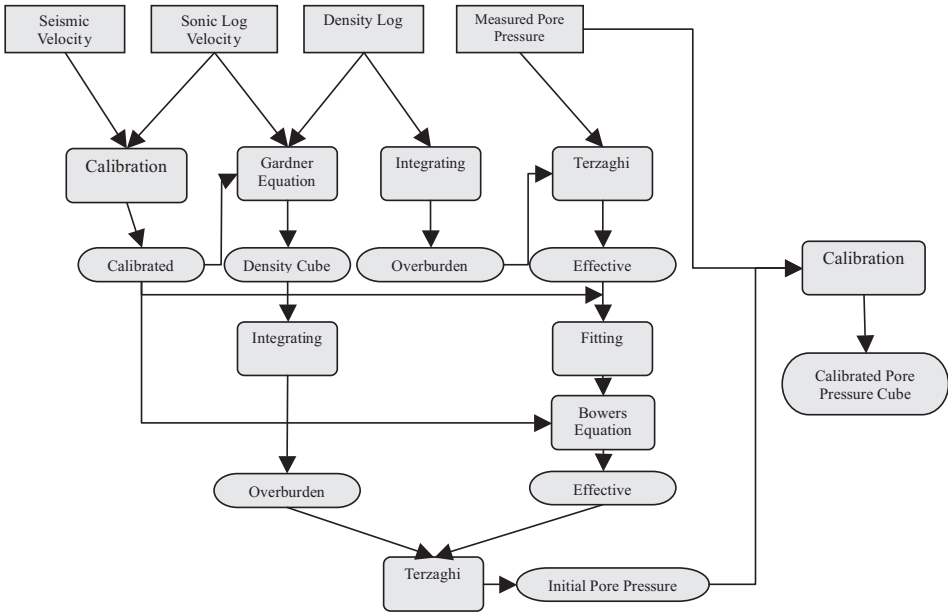
Fig. 1. The overall flow-diagram for pore pressure prediction in this study.

Data preparation

The available rms velocity was converted to the interval velocity using Dix formula. The velocity cube was restricted from 0 to 3 s two way time because of the maximum depth of the wells. The average velocity is about 4000 m/s in this area. So, the restricted cube would cover around 6000 m depth which is enough for oil fields in Iran. For converting the depth scale to a two way time scale and vice versa, a relationship was fitted to the check-shot data for each well. To eliminate the effects of high frequencies on sonic logs (Snijder et al., 2002), a running average technique was applied on sonic logs with 50 m. Finally, the measured pressure data at wells were converted into two-way time scale using the check-shot relationship.

Seismic velocity calibration

Pore pressure prediction needs an accurate velocity field (Cibin et al., 2004). The seismic velocity is based on processing methods and may be different from the geological based velocity. The seismic velocity field is

generally derived either from the stacking velocities or from prestack migration analyses. The stacking velocity lacks vertical and horizontal resolution; therefore, it can be applied for pore pressure prediction only if the geological and lithological models are not too complex and dips are almost negligible (Lee et al., 1999). The prestack time migration velocity can partially compensate for model complexities. Both types of velocities can be used quite successfully where the theoretical conditions for the application of Dix formula are valid. However, the density of the picked velocity functions is important for the lateral details (Cibin et al., 2004). In this study, for improving the resolution of the velocity field and for correcting the seismic velocity with regard to geology, a geostatistical calibration process has been applied to increase the correlation between the seismic velocity and velocities derived from the sonic logs. By calculating the seismic velocity at locations of wells, using a geostatistical interpolation method (kriging), the velocity calibration parameters will become available at the wells.

Before running kriging on the initial seismic velocity, a variography was carried out (Chambers et al., 2000). Variography is a spatial statistical tool for detecting the varieties in different direction in the 2D or 3D space. Varigraphy is necessary for determining the basic parameters of Kriging or other geostatistical methods. Variography was done both omni-directionally and directional in five different directions (Fig. 2). As expected, the omni directional and the vertical variograms do not reach their sills as a result of increasing velocity with depth and the existing trend (Hohn, 1998). The range, sill and nugget effect parameters which are extracted from these variograms are shown in Table 1. The nugget effect shows the small scale varieties which are not detectable in the variogram scale. So, they would be appeared as intersection in variogram curves. The range shows the maximum distance between the two samples when they are statistically dependent. Also, the sill shows the maximum value of variogram which it is equal to the ordinary variance between samples. The fitted model to the vertical variogram is Gaussian which shows a high level of continuity of velocity as a regional variable (Hohn, 1998). The results of the variography show that the lateral variation of the seismic velocity is low and the Dix formula is satisfied. The search radius of the kriging is selected using these variograms.

Seismic velocities were calculated at the well-locations using the kriging method. The differences between velocities derived from the sonic logs and seismic velocities were calculated at the well-locations. The results are the sample-by-sample velocity calibration parameters at the well-locations. For interpolating these parameters in the velocity cube and calibrating the seismic velocity with regard to velocities derived from the sonic logs, the variograms of these parameters are needed. Table 2 shows the extracted parameters from these variograms. The long distances between wells lead to almost large nugget effects (Hirsche et al., 1998).
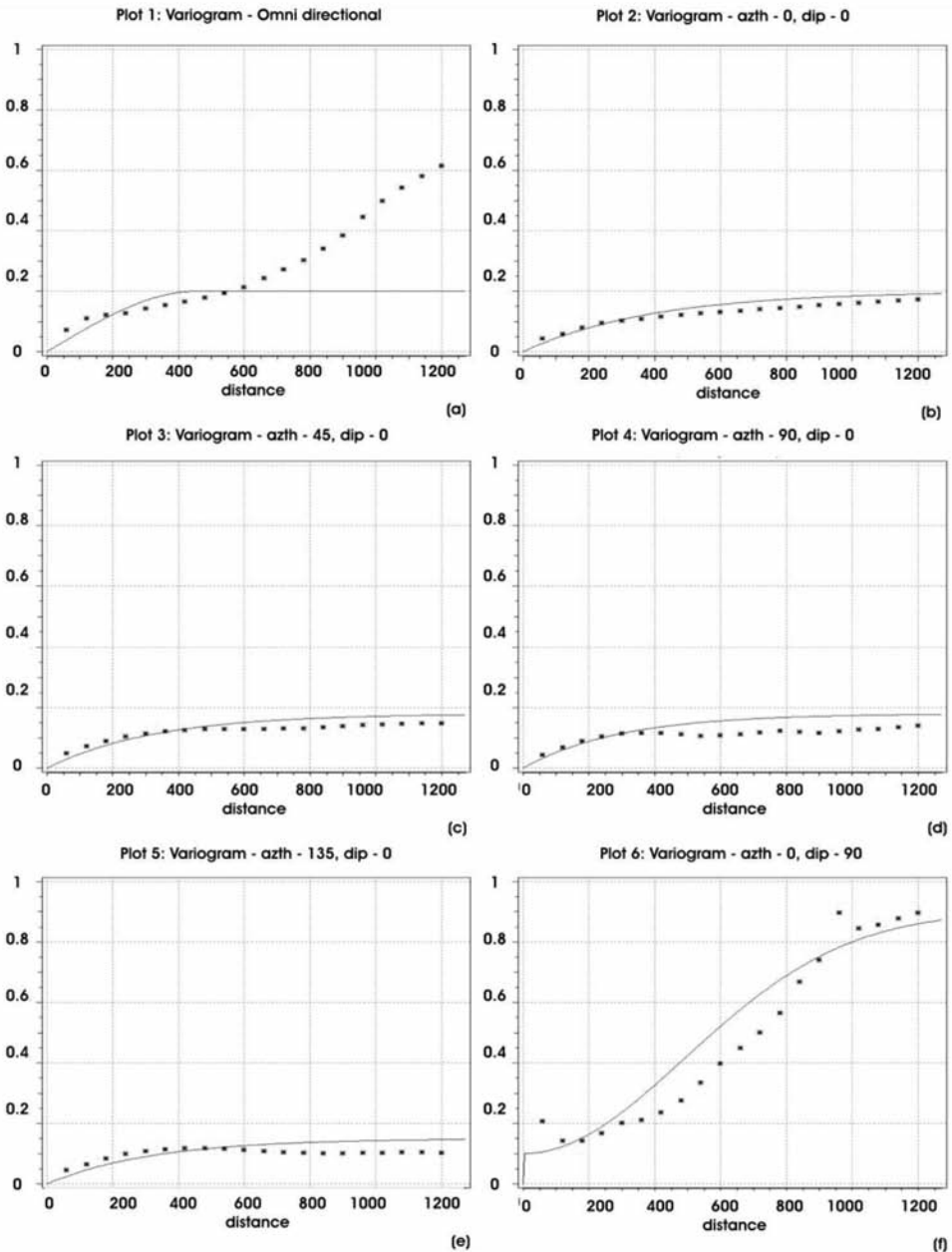
Fig. 2. The variograms of initial seismic velocity: (a) Omni-directional variogram. (b) Variogram at dip 0° and azimuth 0°. (c) Variogram at dip 0° and azimuth 45°. (d) Variogram at dip 0° and azimuth 90°. (e) Variogram at dip 0° and azimuth 135°. (f) Variogram at dip 90° and azimuth 0°. The solid line is the fitted spherical model to experimental variogram and used for extracting the parameters of Kriging. In (a) the poor fit is due to vertical increase in velocity with depth. This effect is out of the layer thickness and is not effective in this estimation.

Table 1. Extracted parameters from the variograms of the initial seismic velocity.

Azimuth (degree)	Dip (degree)	Fitted model	Range	Sill	Nugget effect
Omni directional	Omni directional	Spherical	15000 m	0.2	0
0	0	Spherical	20000 m	0.2	0
45	0	Spherical	20000 m	0.18	0
90	0	Spherical	20000 m	0.18	0
135	0	Spherical	20000 m	0.17	0
0	90	Gaussian	1000 ms	0.9	0

Table 2. Extracted parameters from the variograms of the velocity calibration parameters at the well-locations.

Azimuth (degree)	Dip (degree)	Fitted model	Range	Sill	Nugget effect
Omni directional	Omni directional	Spherical	20000 m	1.1	0.5
0	0	Spherical	20000 m	0.8	0.5
45	0	Spherical	20000 m	0.85	0.5
90	0	Spherical	20000 m	0.9	0.5
135	0	Spherical	20000 m	0.8	0.5
0	90	Spherical	425 ms	1.1	0.5

Parameters of velocity calibration at the well-locations were interpolated on the initial picked velocity-locations. Note that the well logs are not available in complete depth-range of the velocity cube, so the velocity calibration parameter, and the most upper and the lower parts of the cube are not affected by the velocity calibration process. After that, the calibrated seismic velocity with regard to the velocities derived from sonic logs would be available at the main velocity analysis locations. This method is suitable for large oil fields with a few wells, where a lateral change in the parameters is expected (Kelly et al., 2005). A regular grid size which is specified in Table 3 was used to sort the distribution of the velocity in this area. If the distance between the estimation points is very short, the results of the estimation at adjacent points will be similar to each other (Hirsche et al., 1998). In many studies, the resolution of the PSTM grid is sufficient for an accurate pore pressure prediction (Clarembaux et al., 2005). However, in this study, as a result of an irregular velocity network and low resolution of the stacking velocity, the velocity grid sorting has been done using a geostatistical interpolation method. The results of the kriging of the calibrated seismic velocity on a regular grid are shown in Fig. 3. The horizontal resolution of the final grid size is 250 by 250 m and the vertical resolution is 30 ms.

Table 3. Estimation grid used for sorting of the seismic velocity grid and predicting pore pressure.

Direction	Number of estimation points	Estimation point spacing
X	188	250 m
Y	220	250 m
z (twt)	100	30 ms

After velocity calibration and sorting, the cross-validation of the final velocity cube for checking the accuracy of the seismic velocity with regard to well-derived velocities is carried out. For this purpose, the cross-plots of the seismic velocity and the velocity derived from sonic logs versus two-way time at the well-locations were used (Fig. 4). This figure shows that the results of the calibrating- and the sorting process are acceptable. The frequency differences between seismic traces and well logs are taken into account: the moving average technique was implemented to eliminate the effect of high frequencies on well logs; viz. a high cut-filter was applied.
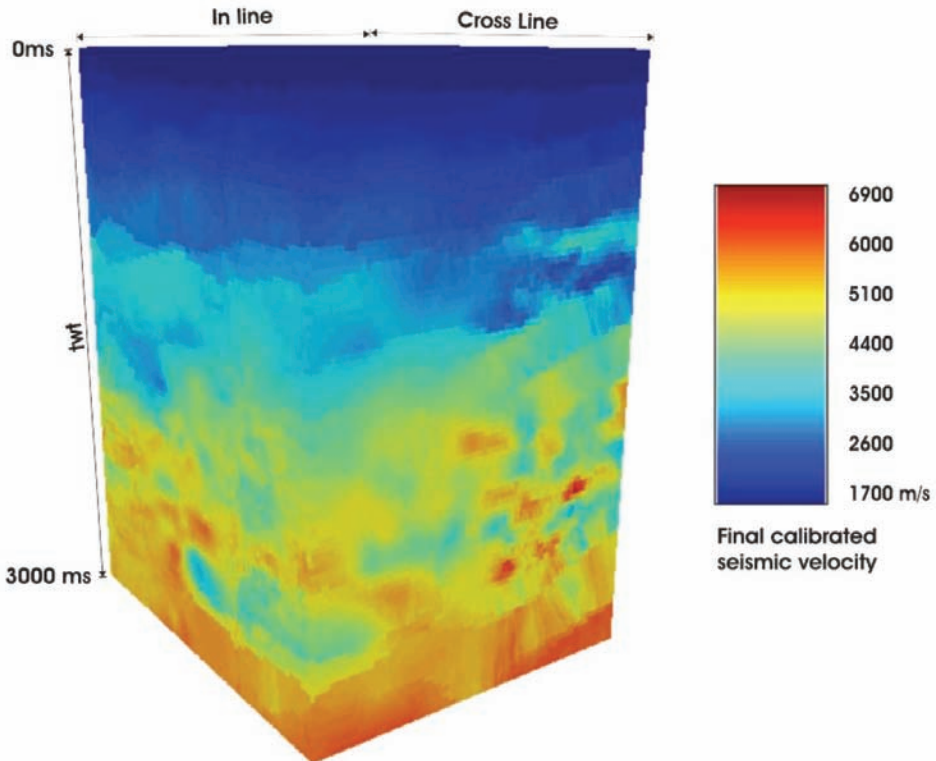

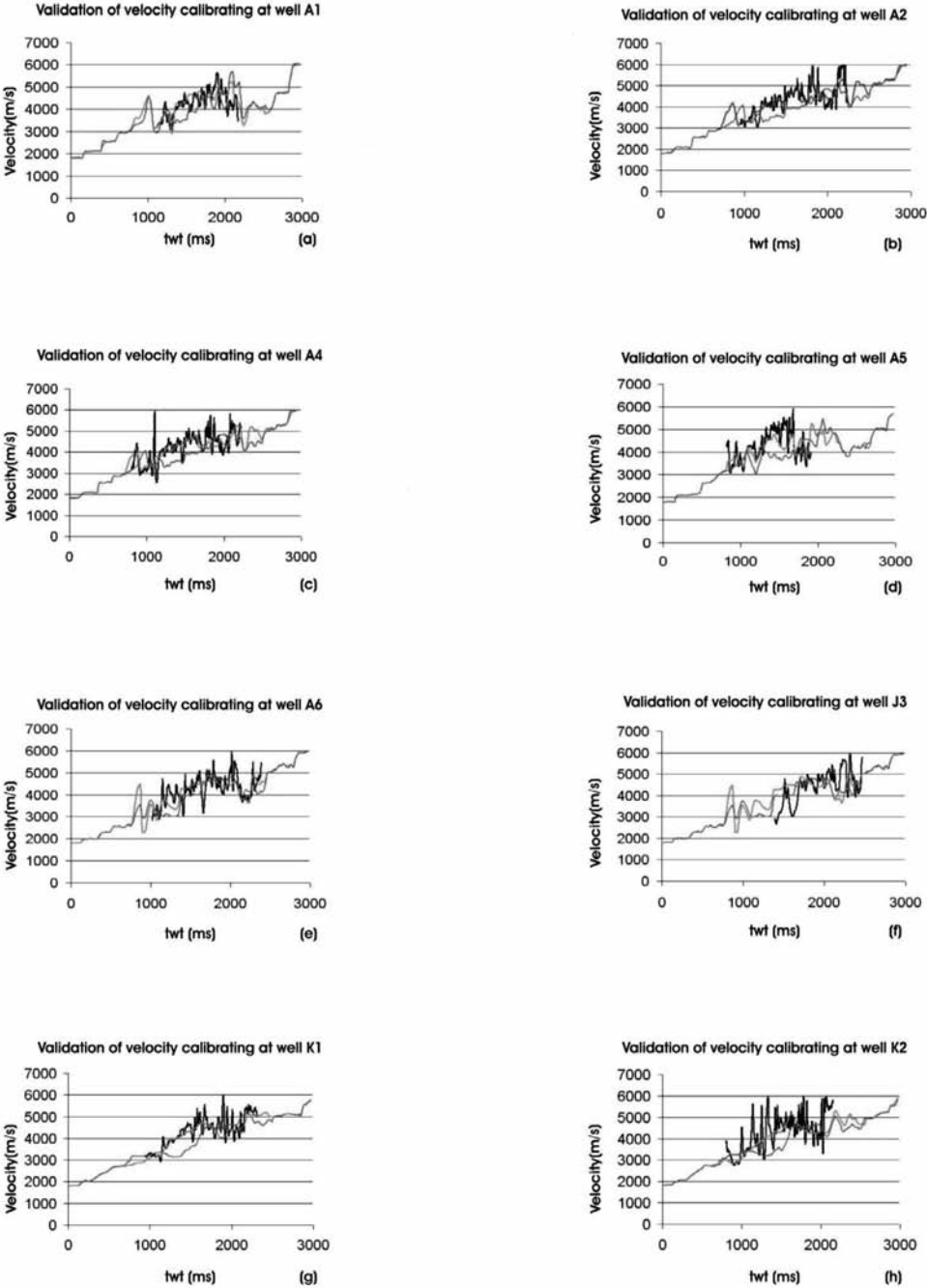Fig. 3. The final calibrated and sorted seismic velocity cube.

Validation of velocity calibrating at well A1

Validation of velocity calibrating at well A2

Validation of velocity calibrating at well A4

Validation of velocity calibrating at well A5

Validation of velocity calibrating at well A6

Validation of velocity calibrating at well J3

Validation of velocity calibrating at well K1

Validation of velocity calibrating at well K2

Fig. 4. The validation of the velocity calibration procedure with regard to the velocities derived from the sonic logs. The thick black line shows the well velocity, the blue line shows the uncalibrated seismic velocity and the red line is the final calibrated seismic velocity.

Overburden pressure calculation

The effective pressure is needed to fit the Bowers equation at the well-locations. The pore pressure was measured at the locations of the wells. So, if the overburden pressure was available at the well-locations, the effective pressure would be available. By integrating the density logs at the well-locations, eq. (1), the overburden pressure was calculated (Sayers et al., 2002):

$$S_V(Z) = g \int_0^Z \rho(Z)dZ \ , \tag{1}$$

where $S_V(Z)$ is the overburden pressure at depth Z, is the gravitational acceleration of the earth, and $\rho(Z)$ is the rock density at depth Z. After calculating the overburden pressure, the effective pressure was calculated using eq. (2).

$$\sigma_V = S_V - p \ , \tag{2}$$

where σ_V is the effective pressure, and p is the pore pressure. In eq. (1), integration should be made with regard to the depth. So, the cumulative integration for each well was made using density logs in the depth-range of interest. The calculated overburden pressures at each well were converted to two-way time scale using the check-shot data.

Effective pressure calculation

The pore pressures were measured at each well using RFT/DST tests. After calculating the overburden pressures at each well, using eq. (2) the effective pressures were calculated using the measured pore pressure and the calculated overburden pressure. Then, the cross-plot of the calibrated seismic velocity versus the calculated effective pressure at the well-locations was used for fitting Bowers equation (Fig 5). This figure shows that in contrast to sandstone reservoirs, the correlation between the effective pressure and the seismic velocity is weak for carbonate reservoirs. The Bowers equation (1995) is:

$$V = V_0 + A\sigma_V^B \ , \tag{3}$$

where V is the seismic velocity at a specified depth, V_0 is the seismic velocity at zero effective pressure (surface), σ_V is the effective pressure at the specified depth, A and B are coefficients of the Bowers equation. In Fig. 5, the magnitude of the $V - V_0$ was plotted versus the effective pressure to simplify

fitting the Bowers equation. The V0 was selected 1800 m/s using available seismic data. After fitting the Bowers equation, "A" and "B" coefficients were selected and the final Bowers eq. was calculated as:

$$V = 1800 + 41.65\sigma_V^{0.4783} \quad . \tag{4}$$

Because of the extension of the area, before using eq. (4), the coefficients of the Bowers equation were calculated separately for each well. Eq. (4) was selected as the final Bowers equation.
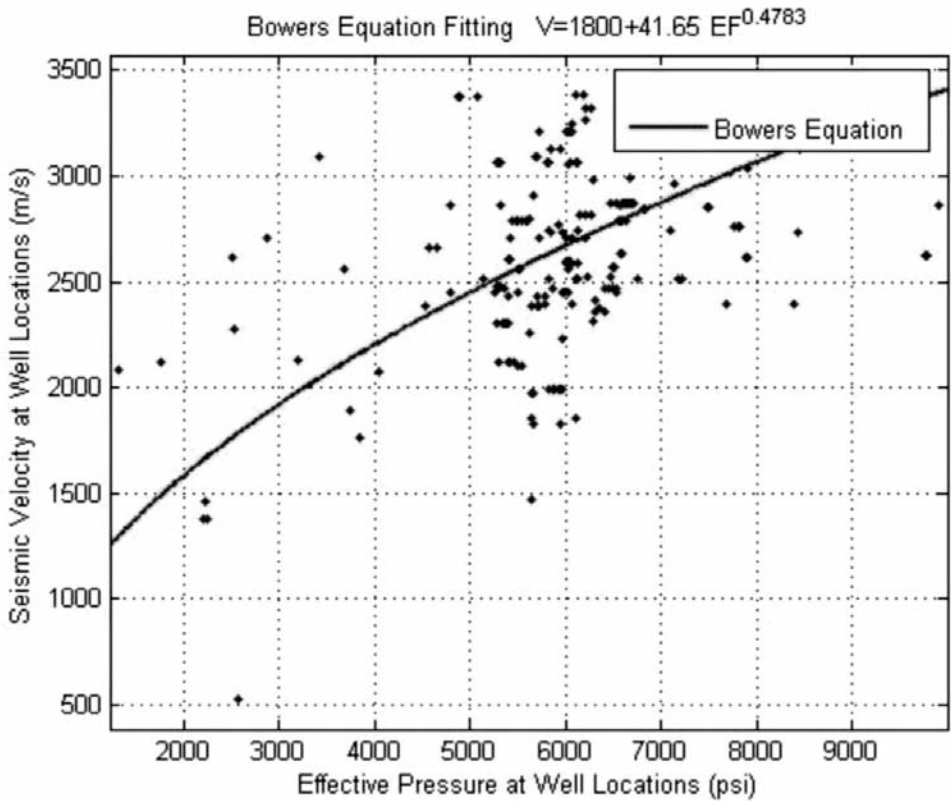

Fig. 5. The cross-plot of the effective pressure versus the seismic velocity. For better fitting of the Bowers equation, $V - V_0$ has been plotted versus the effective pressure. V_0 is the velocity at the zero effective pressure, which is equal to 1700 m/s in this area.

Density cube calculation

Calculating the pore pressure requires to have available the overburden pressure and the effective pressure. The overburden pressure cube calculation needs the density cube. For preparing the density cube the Gardner (1974)

relationship was used to convert the calibrated seismic velocity cube to the density cube. The coefficients of the Gardner equation (1974) were determined through fitting this relationship to density-velocity data at each well which are derived from well logs. After calculating the coefficients of the Gardner relationship, the velocity cube was converted to density cube. The Gardner equation is defined as:

$$\rho = aV^b \quad , \tag{5}$$

where ρ is the density in g/cm³, V is the velocity, and a, b are Gardner coefficients. When well data were not available a, b were assumed to be 0.25. In this study, the coefficients of the Gardner equation were calculated using well log data. The cross-plot of the velocities derived from well logs and the density logs are shown in Fig. 6. The coefficients of the Gardner equation were calculated as follows:

$$\rho = 0.3196V^{0.2450} \quad . \tag{6}$$

According to eq. (6) the calibrated velocity cube was converted to the density cube.
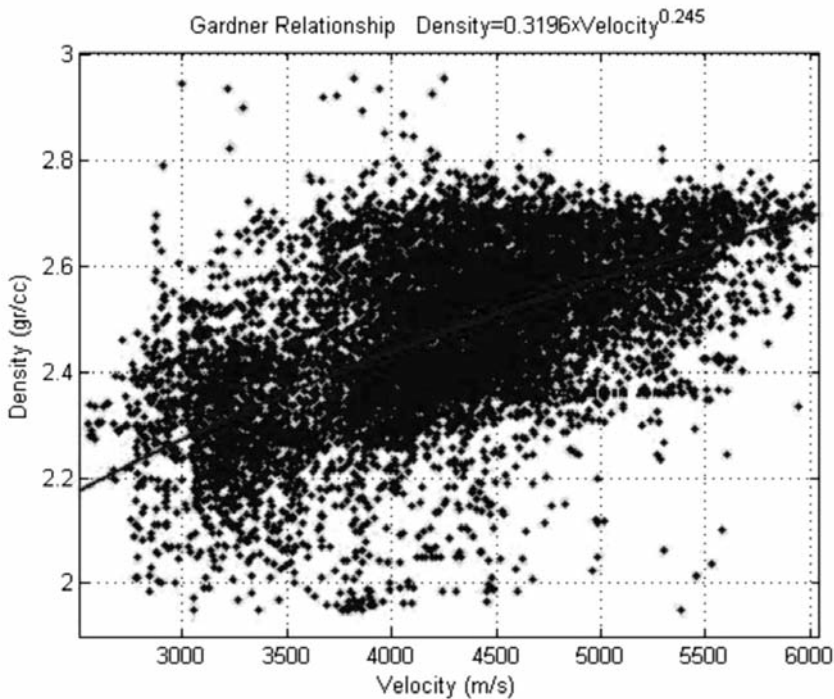

Fig. 6. The cross-plot of the velocity versus density, which is measured at the 8 wells, and the fitted Gardner equation.

Pressure cube calculation

The overburden pressure cube was calculated in the same manner as the overburden pressure at each well. The integration was done for each point at the surface of the density cube as well as the density logs for each well. In this procedure, eq. (1) was used again for calculating the overburden pressure cube. After that, the calibrated velocity cube was converted to the effective pressure cube using eq. (4). Fig. 7 shows the effective pressure cube. The grid size of the overburden pressure cube and the effective pressure cube was the same. So, the initial pore pressure could be calculated by calculating the difference between the overburden pressure and the effective pressure for each grid point. Final results would be the initial pore pressure cube (Fig. 8). According to the weak correlation observed between the velocity and the effective pressure in Fig. 5, the initial pore pressure cube was not of sufficient resolution and therefore the estimated pore pressure cube was underestimated. To improve the accuracy and the resolution of the pore pressure cube, geostatistical calibration parameters were estimated using the initial pore pressure cube with regard to the measured pore pressure at each well.
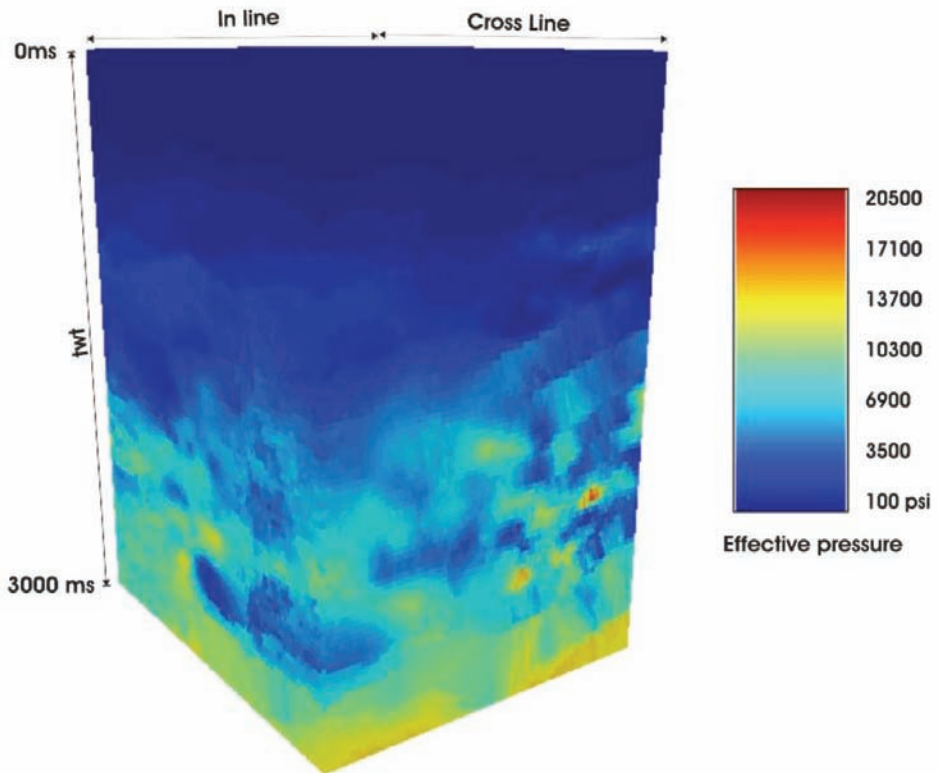

Fig. 7. The effective pressure cube which was constructed using the Bowers equation.

Geostatistical pore pressure calibration

An additional calibration step was needed to compensate for the weak correlation between the effective pressure and the seismic velocity in these carbonates. Calibrating the initial pore pressure with regard to the measured pore pressure at each well led to a significant improvement of the resolution of the final pore pressure cube (Snijder et al., 2002). The geostatistical calibration procedure, used in this step, is the same as the velocity calibration process. However, because of the regular grid of the initial pore pressure, a sorting step was not needed in this step. The initial pore pressure (Fig. 8) was extracted at the locations of the wells. The differences between the predicted pore pressure and the measured pore pressure at each well were used to calculate the pore pressure calibration parameters. This procedure estimates the pore pressure calibration parameters at each well. Then, the variograms of these calibration parameters were calculated in the same way as the variograms of the velocity calibration parameters. After extracting kriging parameters, the pore pressure calibration parameters were interpolated at the initial pore pressure cube.
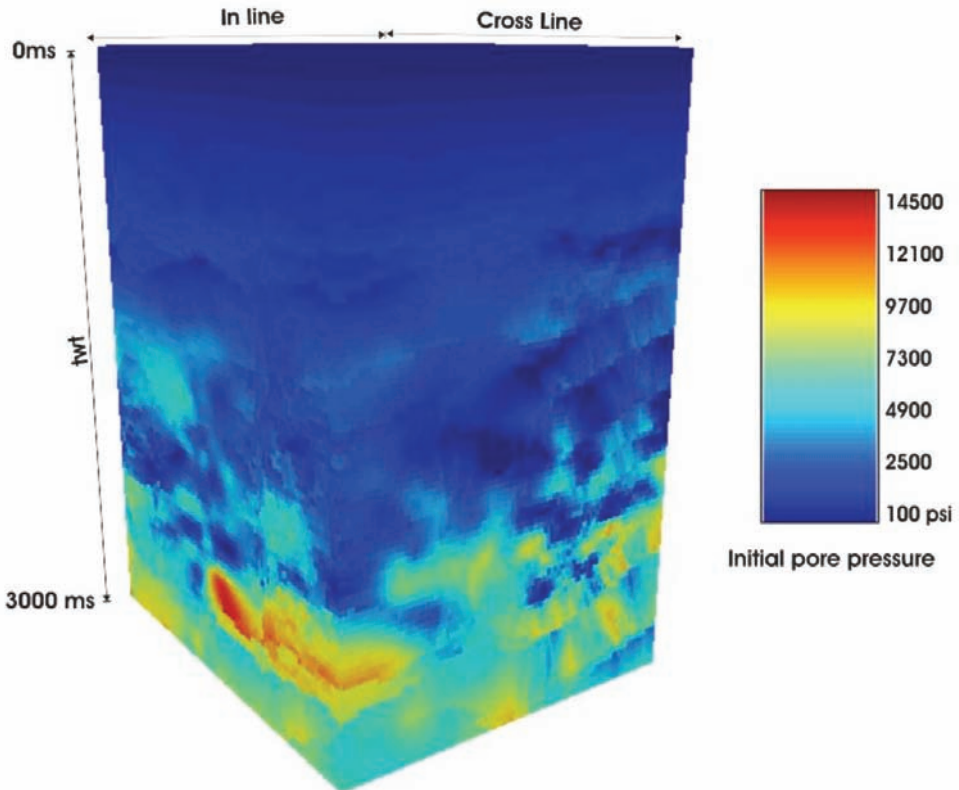

Fig. 8. The initial pore pressure cube.

The extracted variogram parameters are shown in Table 4. As a result of the short range of the vertical variogram, the search radius of the kriging is small in the vertical direction. The calibrated pore pressure cube was calculated by adding the initial pore pressure and the calibration parameters at each point of the grid (Fig. 9). This figure shows pressures with higher resolution than the initial pore pressure cube (Fig. 8).

Table 4. Extracted parameters from the variograms of the pore pressure calibration parameters at the well-locations.

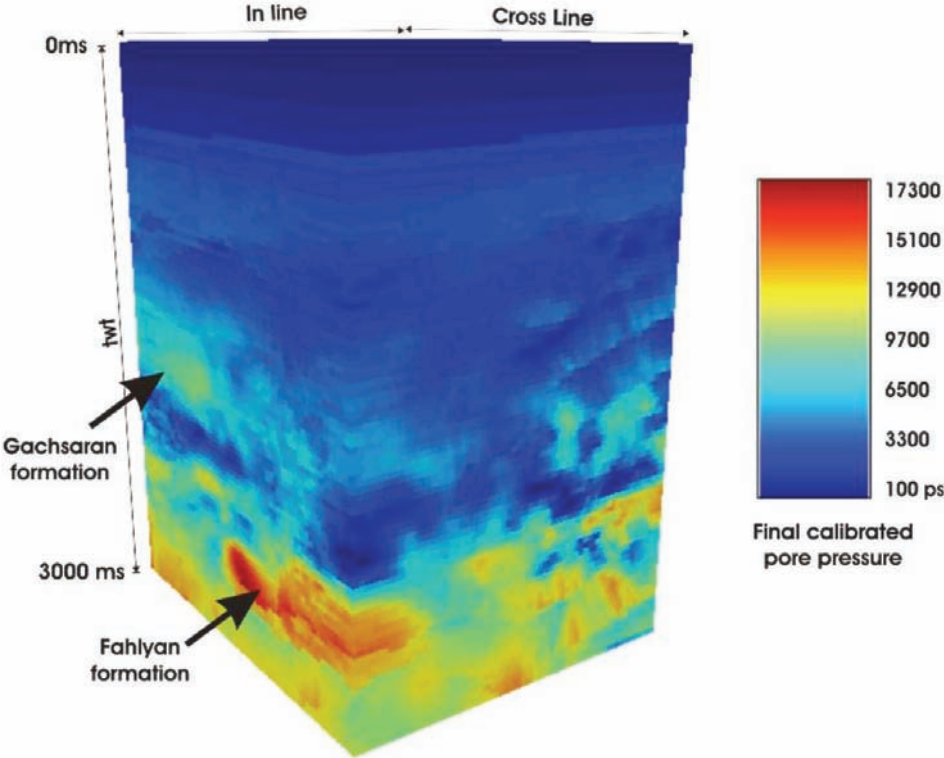| Azimuth (degree)	Dip (degree)	Fitted model	Range	Sill	Nugget effect
Omni directional	Omni directional	Spherical	10000 m	1	0.2
0	90	Spherical	200 ms	1	0

Fig. 9. The final calibrated pore pressure cube.

Validation of the predicted pore pressure

For validating the accuracy of the final predicted pore pressure cube, the predicted pore pressure was extracted at all well locations. Fig. 10 shows the predicted pore pressures (grey line) and measured pore pressures (black dots) versus two-way time for each well. This figure verifies that the predicted pore pressures have acceptable accuracy for drilling purposes.

DISCUSSION

The geological interpretation of the final calibrated pore pressure cube for finding stratigraphic traps, investigating the hydrodynamic regime of faults, investigating seal integrity, and planning of wells has significant effects on the interpretation of the exploration data. This study shows that applying the pore pressure prediction using the seismic velocity is possible in carbonate formations. However, because of the differences between the properties of the
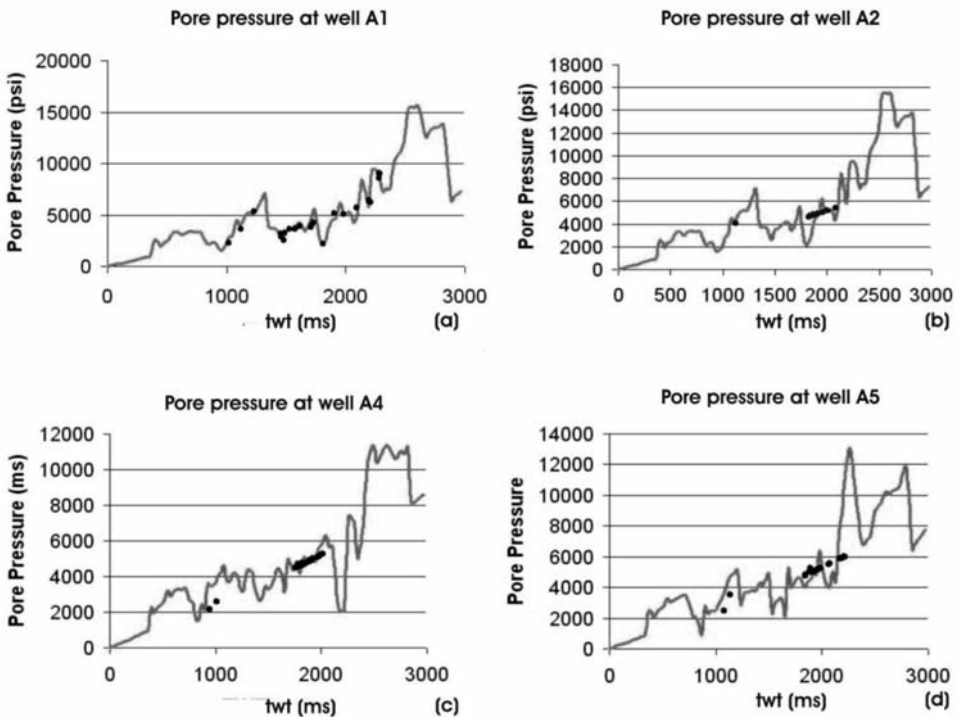

Fig. 10(a)-(d). The predicted pore pressures at the well-locations (red lines) and the measured pore pressures at the well-locations (black dots).

carbonate and sandstone rocks, the results for carbonates will be weaker than those of sandstones. In carbonate rocks, the Bowers equation (1995) considers different processes for the occurrence of overpressure zones leading to better results as compared to the Eaton equation (1975) which considers the shale as the main reason for overpressure formations. In addition, Fig. 6 shows a decreasing trend is detectable on the density-velocity cross-plot. This means that no unloading process exists in this area and the common Bowers eq. is enough for predicting the pore pressure. The process of tectonical unloading in the area leads to a robust decrease in the general trend of the density-velocity cross-plot. It means that an improved Bowers equation needs to convert the seismic velocity to the accurate effective pressure. Furthermore, the results show that the geostatistical calibration and correction methods used in this work can be used for achieving accurate velocity fields for processing and imaging purposes, in agreement with Lee and Xu (2000). We recommend the application of the proposed new relationships in pore pressure prediction studies rather than using laboratory test data.
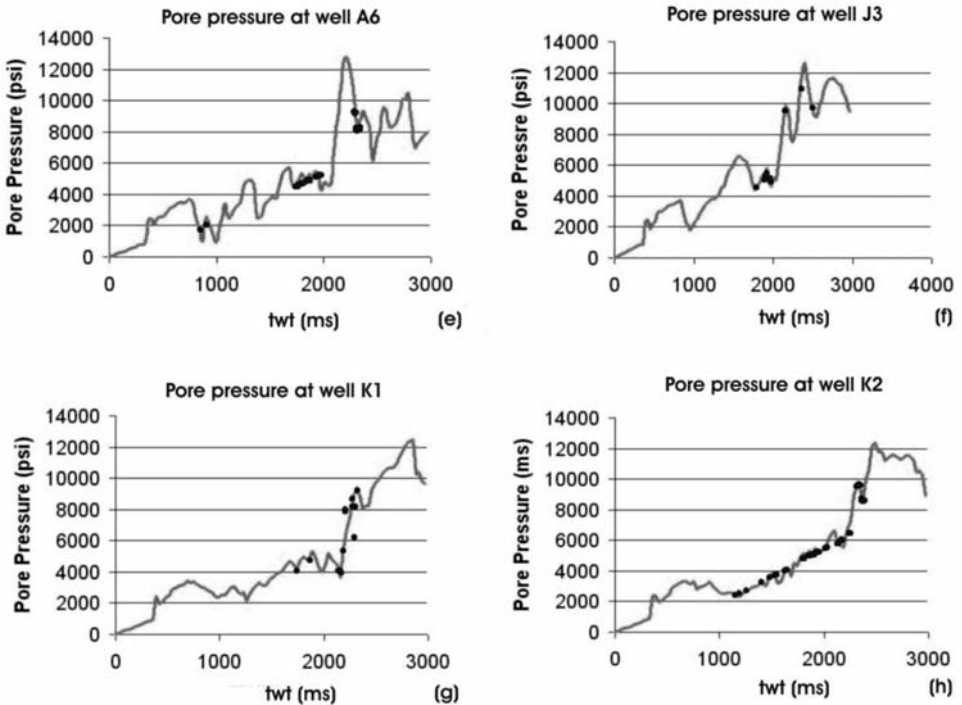

Fig. 10(e)-(h). The predicted pore pressures at the well-locations (red lines) and the measured pore pressures at the well-locations (black dots).

CONCLUSIONS

The final calibrated pore pressure cube shows that the Fahliyan carbonate formation encounters clearly abnormal pore pressure zones. Several explanations are possible for this phenomenon. The most probable explanation may be the large depth of burial of this formation and the conversion of heavy oil to lighter products and gas. Inversion of seismic impedance shows that the Fahliyan formation has many reef structures that could have influences on constructing isolated abnormal pressure zones. These reef structures could act as isolated structures at some parts of the field, where the overlying formation has contains shale lithology. The lateral lithology variation, which was detected in this formation, may have influences on pressure changes. This phenomenon leads to the high pressure pockets at the Fahliyan formation.

The final calibrated pore pressure cube has significantly less resolution in some parts of the field, where the available velocity field was the stacking velocity (e.g., around well K2). In addition to the low-resolution velocity field, the limited number of wells led to a smoother pore pressure cube in this part of the field. These results show that the overpressure danger is a serious problem for drilling the Fahliyan formation and for developing this oil field. The results of the velocity calibration show that the calibrated velocity is in good agreement with the measured velocities at the well-locations. In addition, the resolution of the calibrated velocity is significantly improved over the uncalibrated seismic velocity. In this study, the lack of sufficient resolution of the pore pressure cube is related to the low resolution velocity field. So, an additional geostatistical calibration process was proposed to improve the resolution of the pore pressure cube. This process calibrates the predicted pore pressure with the measured pore pressures at the well-locations. Finally, the final calibrated pore pressure cube has enough resolution for the planning of wells and the prediction results are in good agreement with the measured pore pressure at the well-locations.

ACKNOWLEDGEMENTS

REFERENCES

Badri, M.A., Sayers, C.M., Awad, A. and Graziano, A., 2000. A feasibility study for pore-pressure prediction using seismic velocities in the offshore Nile Delta, Egypt. The Leading Edge, 19: 1103-1108.

Bowers, G.L., 1995. Pore pressure estimation from velocity data: Accounting for pore pressure mechanisms besides undercompaction. SPE Drilling and Completion, 10: 89-95.

Carcione, J.M. and Helle, H.B., 2002. Rock physics of geopressure and prediction of abnormal pore fluid pressures using seismic data. CSEG Recorder, 27, 7: 9-30.

Chambers, R.L., Yarus, J.M. and Hird, K.B., 2000. Petroleum geostatistics for nongeostatisticians, Part 1. The Leading Edge, 19: 474-479.

Chopra S. and Huffman, A., 2006. Velocity determination for pore pressure prediction. CSEG Recorder, 31, 4: 28-44.

Cibin, P., Martera, M.D., Buia, M., Calcagni, D., Runcer, D.J. and Talkan, T., 2004. What seismic velocity field for pore pressure prediction? Expanded Abstr., 74th Ann. Internat. SEG Mtg., Denver: 1531-1534.

Clarembaux, J.C., Giusso, M., Gullco, D., Miranda, C.C., Leiva, J.G.L. and Altamirano, S.A.S., 2005. Seismic pore pressure prediction without well data and poorly defined normal compaction trend lines. A case study from the Rio Bravo delta, northern Mexico. Expanded Abstr., 75th Ann. Internat. SEG Mtg., Houston: 1227-1231.

Den Boer, L.D., Sayers, C.M., Nagy, Z.R., Hooyman, P.J. and Woodward, M.J., 2006. Pore pressure prediction using well-conditioned seismic velocities. First Break, 24: 43-49.

Dodds, K.J., Dewhurst, D.N., Siggins, A.F., Ciz, R., Urosevic, M., Gurevich, B. and Sherlock, D.H., 2007. Experimental and theoretical rock physics research with application to reservoir, seals and fluid processes. J. Petrol. Sci. Engin. 57: 16-36.

Dutta, N., Mukerji, T., Prasad, M., and Dvoorkin, J., 2002, Seismic detection and estimation of overpressures part II: field applications. CSEG Recorder, 27, 7: 58-72.

Eaton, B.A., 1975. The eq. for geopressure prediction from well logs. SPE 5544.

Gregory, A.R., 1978. Aspects of rock physics from laboratory and log data that are important to seismic interpretation. In: Payton, C.E. (Ed.), Seismic Stratigraphy-Applications to Hydrocarbon Exploration. AAPG, Memoir 26, Tulsa, OK: 15-46.

Hirsche, K., Boerner, S., Kalkomey, C. and Gastaldi, C., 1998. Avoiding pitfalls in geostatistical reservoir characterization. A survival guide. The Leading Edge, 17: 493-504.

Hohn, M.E., 1998. Geostatistics and Petroleum Geology. Kluwer Academic Publishers, Dordrecht, Netherlands.

Kan, T.K., Kilsdonk, B. and West, C.L., 1999. 3-D geopressure analysis in the deepwater Gulf of Mexico. The Leading Edge, 18: 502-508.

Kan, T.K. and Swan, H.W., 2001. Geopressure prediction from automatically-derived seismic velocities. Geophysics, 66: 1937-1946.

Kelly, M.C., Skidmore, C.M. and Cotton, R.D., 2005. Pore pressure prediction for large surveys. Expanded Abstr., 75th Ann. Internat. SEG Mtg., Houston: 1239-1243.

Lee, S., Shaw, J., Ho, R., Burger, J., Singh, S. and Troyer, B., 1999. Illuminating the shadows: tomography, attenuation and pore pressure processing in the South Caspian Sea, J. Petrol. Sci. Engin., 24: 1-12.

Lee, W.B. and Xu, W., 2000. 3-D geostatistical velocity modeling: Salt imaging in geopressured environment. The Leading Edge, 19: 32-36.

Sayers, C.M., Johnson, G. M. and Denyer, G., 2002. Predrill pore pressure prediction using seismic data. Geophysics, 67: 1286-1292.

Snijder, J., Dickson, D., Hillier, A, Litvin, A., Gregory, C. and Crookall, P., 2002. 3D pore pressure prediction in the Columbus basin, offshore Trinidad & Tobago. First Break, 20: 283-286.